Inorg. Chem. **2009**, *48*, 164−173

Synthesis and Spectroscopic and Electrochemical Studies of Pyrazine- or Pyridine-Ring-Fused Tetraazachlorins, Bacteriochlorins, and Isobacteriochlorins

Elena A. Makarova,[†] Ekaterina V. Dzyuina,[†] Takamitsu Fukuda,[‡] Hironori Kaneko,[‡] Naoaki Hashimoto,[‡] Yuu Kikukawa,[‡] Nagao Kobayashi,*[,‡] and Evgeny A. Lukyanets*[,†]

Organic Intermediates and Dyes Institute, B. Sadovaya 1/4, Moscow 123995, Russia, Department of Chemistry, Graduate School of Science Tohoku University, Sendai 980−8578, Japan

Received August 14, 2008

Mixed condensation of tetramethylsuccinonitrile and either 2,3-dicyano-5,6-diethylpyrazine, 2,3-dicyanopyridine, or 3,4-pyridinedicarboximide in the presence of nickel chloride forms novel pyrazine-, 2,3-pyridine-, or 3,4-pyridine-ring-fused tetraazachlorin (TAC), tetraazabacteriochlorin (TABC), and tetraazaisobacteriochlorin (TAiBC) derivatives. All possible structural isomers were separated using repeated thin-layer chromatography and have been investigated by absorption and magnetic circular dichroism spectroscopy. Similarly to previously reported TAC analogues, the TAC and TABC derivatives show large splitting of the Q band, while a single, intense absorption band is observed for the TAiBC derivatives. Although the absorption spectra are practically identical in shape for the separated structural isomers of TACs and TABCs, the Q-band maxima of the TAiBCs depend significantly on their structures. The observed spectroscopic properties were interpreted on the basis of electrochemical data and the results of (time-dependent) DFT calculations.

Introduction

Skeleton-hydrogenated tetraazaporphyrin (TAP, or porphyrazine) analogues, namely, tetraazachlorins (TACs), tetraazabacteriochlorins (TABCs), and their structural isomers, tetraazaisobacteriochlorins (TAiBCs), depending on the numbers and location of the β-hydrogenated pyrrole units, are currently attracting considerable attention, since the structurally analogous hydrogenated porphyrin derivatives have been widely studied as photosensitizers for photodynamic cancer therapy (PDT; Scheme 1).[1] The electronic structures of hydrogenated TAP analogues are, however, more similar to those of phthalocyanine (Pc) derivatives than porphyrins because the four *meso*-nitrogen atoms instead of methine carbons cause sizable stabilization of the HOMO−1 energy level, which leads to large absorption coefficients in the visible to near-infrared region.[2] These spectroscopic features are advantageous for absorbing living-tissue-permeable light and, as a consequence, for generating active singlet oxygen more effectively. Therefore, hydrogenated TAP derivatives are attractive materials as next-generation photosensitizers. The first synthesis of TAC derivatives was attempted in 1958 by Linstead et al., by employing catalytic hydrogenation of the corresponding TAP derivatives.[3] How-

Scheme 1. General Structure of TAC (left), TABC (middle), and TAiBC (right)

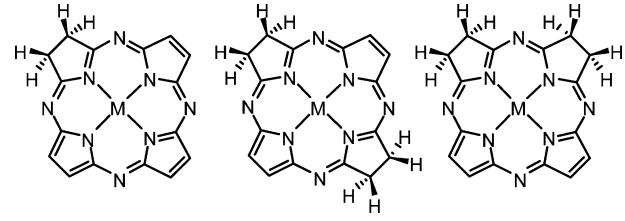

* Authors to whom correspondence should be addressed. Fax: (+81)22-795-7719 (N.K.), (+7)495-254-1200 (E.A.L.). E-mail: nagaok@mail.tains.tohoku.ac.jp (N.K.), rmeluk@niopik.ru (E.A.L.).
† Organic Intermediates and Dyes Institute.
‡ Graduate School of Science Tohoku University.

(1) (a) Pandey, R. K.; Zheng, G. In *The Porphyrin Handbook*; Kadish, K. M., Smith, K. M., Guilard, R., Eds.; Academic Press: San Diego, CA, 2000; Vol. *6*, Chapter 43. (b) Okura, I. *Photosensitization of Porphyrins and Phthalocyanines*; Kodansha: Tokyo, 2000. (c) Lang, K.; Mosinger, J.; Wagnerova, D. M. *Coord. Chem. Rev.* **2004**, *248*, 321. (d) Fukuda, T.; Kobayashi, N. *Dalton Trans.* **2008**, *4685*.

(2) Gouterman, M. *J. Mol. Spectrosc.* **1961**, *6*, 138.

(3) Ficken, G. E.; Linstead, R. P.; Stephen, E.; Whalley, M. *J. Chem. Soc.* **1958**, 3879.

10.1021/ic801552u CCC: $40.75
Published on Web 12/02/2008

ever, these hydrogenated compounds were too unstable to be isolated and characterized, and it is known today that their characterizations were incorrect.[1d] Recently, our group has succeeded in obtaining chemically stable TAC derivatives by employing Diels−Alder addition of dienophiles to the TAP skeleton or by using tetramethylsuccinonitrile as a source of the hydrogenated sites.[4−8] These methodologies enabled us to isolate and fully characterize the TAC, TABC, and TAiBC skeletons, and their benzo-, 2,3-naphtho-, or 1,2-naphtho-fused derivatives. Our group has also reported C_{60}-containing TAC, TABC, and TAiBC derivatives, in which 1,2-dicyanofullerene was employed as the source of the hydrogenated sites, and proved that these conjugates show large molecular orbital (MO) interactions between the constituting units.[9,10]

Herein, we report the synthesis and isolation of all of the possible isomers of novel 2,3-pyrazino-, 2,3-pyridino-, or 3,4-pyridino-fused TACs, TABCs, and TAiBCs as a new family of hydrogenated derivatives of TAP (or Pc). Although pyrazine- or pyridine-ring containing Pc analogues (pyrazino- or pyridinoporphyrazines) have been reported by several groups, the hydrogenated congeners have not yet been published.[11] The effect of introducing nitrogen atoms is investigated by means of various spectroscopic, electrochemical, and theoretical techniques including UV−vis absorption, magnetic circular dichroism (MCD), cyclic voltammetry (CV), and time-dependent DFT [(TD)DFT] calculations. These nitrogen-containing compounds attract attention as photosensitizers for PDT owing to their higher solubility in aqueous media compared to the previously reported benzo- or naphtho-fused derivatives.

Experimental Section

Measurements and Computational Methods. Absorption, MCD, and cyclic voltammograms were obtained by following the method described in our preceding paper.[8a] High-resolution electron spray ionization Fourier transform ion cyclotron resonance mass spectra were measured with a Bruker APEX III spectrometer. The Gaussian 03 program was used to perform (TD)DFT calculations.[12]

Synthesis and Separations. 2,3-Dicyano-5,6-diethylpyrazine[13] and tetramethylsuccinonitrile[14] were synthesized according to the literature.

Nickel *β,β,β′,β′*-Tetramethyl[tris-2,3-(5,6-diethylpyrazino)]tetraazachlorin (NiTPyz^{Et}TAC, 1), Nickel *β,β,β′,β′,β″,β″,β‴,β‴*-Octamethyl[bis-2,3-(5,6-diethylpyrazino)]tetraazabacteriochlorin (NiDPyz^{Et}TABC, 2), and Nickel *β,β,β′,β′,β″,β″,β‴,β‴*-Octamethyl[bis-2,3-(5,6-diethylpyrazino)]tetraazaisobacteriochlorin (NiDPyz^{Et}TAiBC, 3). A mixture of tetramethylsuccinonitrile (0.78 g, 5.7 mmol), 2,3-dicyano-5,6-diethylpyrazine (0.35 g, 1.9 mmol), and anhydrous $NiCl_2$ (0.46 g, 3.6 mmol) was reacted in the presence of ammonium molybdate in boiling quinoline (5 mL) under argon for 1 h. After cooling to room temperature, the reaction mixture was diluted with 30% aqueous methanol (100 mL). The resulting precipitate was collected by filtration and washed, first with water and then with 30% aqueous methanol. After drying, the crude product was purified and separated by column chromatography (silica, $CHCl_3$). Three colored fractions with R_f values of 0.16, 0.13, and 0.08 were collected and recrystallized from $CHCl_3$/methanol, to give 7 mg (1%) of **2** as a pink solid, 15 mg (2.3%) of **3** as a blue solid, and 84 mg (18%) of **1** as a dark blue solid. HRMS (ESI): *m/z* 775.2959 ([M + Na^+] for **1**); calcd, 775.2963. HRMS (ESI): *m/z* 703.3243 ([M + H^+] for **2**); calcd, 703.3238. HRMS

(4) Makarova, E. A.; Korolyova, G. V.; Tok, O. L.; Lukyanets, E. A. *J. Porphyrins Phthalocyanines* **2000**, *4*, 525.

(5) Miwa, H.; Makarova, E. A.; Ishii, K.; Lukyanets, E. A.; Kobayashi, N. *Chem.−Eur. J.* **2002**, *8*, 1082.

(6) Silva, A. M. G.; Lacerda, P. S. S.; Tome, A. C.; Neves, M. G. P. M. S.; Silva, A. M. S.; Cavaleiro, J. A. S.; Makarova, E. A.; Lukyanets, E. A. *J. Org. Chem.* **2006**, *71*, 8352.

(7) (a) Makarova, E. A.; Korolyova, G. V.; Lukyanets, E. A. *Russ. J. Gen. Chem.* **2001**, *71*, 821. (b) Makarova, E. A.; Korolyova, G. V.; Lukyanets, E. A. *Zh. Obshch. Khim.* **2001**, *71*, 874. (c) Makarova, E. A.; Korolyova, G. V.; Lukyanets, E. A. *Russ. Pat. 2188200* **2002**, *138*, 368675c; C. A. (2003)

(8) (a) Fukuda, T.; Makarova, E. A.; Lukyanets, E. A.; Kobayashi, N. *Chem.−Eur. J.* **2004**, *10*, 117. (b) Makarova, E. A.; Fukuda, T.; Lukyanets, E. A.; Kobayashi, N. *Chem.−Eur. J.* **2005**, *11*, 1235. (c) Makarova, E A.; Dzyuina, E. V.; Lukyanets, E. A. *Russ. J. Gen. Chem* **2006**, *76*, 1165. (d) Makarova, E. A.; Dzyuina, E. V.; Lukyanets, E. A. *Zh. Obshch. Khim.* **2006**, *76*, 1213.

(9) Fukuda, T.; Masuda, S.; Kobayashi, N. *J. Am. Chem. Soc.* **2007**, *129*, 5472.

(10) Fukuda, T.; Masuda, S.; Hashimoto, N.; Kobayashi, N. *Inorg. Chem.* **2008**, *47*, 2576.

(11) (a) Kudrevich, S. V.; van Lier, J. E. *Coord. Chem. Rev.* **1996**, *156*, 163, and references therein. (b) Makhseed, S.; Ibrahim, F.; Samuel, J.; Helliwell, M.; Warren, J. E.; Bezzu, C. G.; McKeown, N. B. *Chem.−Eur. J.* **2008**, *14*, 4810. (c) Donzello, M. P.; Vlola, E.; Cai, X.; Mannina, L.; Rizzoli, C.; Ricciardi, G.; Ercolani, C.; Kadish, K. M.; Rosa, A. *Inorg. Chem.* **2008**, *47*, 3903. (d) Zimcik, P.; Mørkved, E. H.; Andreassen, T.; Lenco, J.; Novakova, V. *Polyhedron* **2008**, *27*, 1368. (e) Makhseed, S.; Ibrahim, F.; Bezzu, C. G.; McKeown, N. B. *Tetrahedron Lett.* **2007**, *48*, 7358. (f) Fogel, Y.; Kastler, M.; Wang, Z.; Andrienko, D.; Bodwell, G. J.; Müllen, K. *J. Am. Chem. Soc.* **2007**, *129*, 11743. (g) Musil, Z.; Zimcik, P.; Miletin, M.; Kopecky, K.; Lenco, J. *Eur. J. Org. Chem.* **2007**, 4535. (h) Bergami, C.; Donzello, M. P.; Ercolani, C.; Monacelli, F.; Kadish, K. M.; Rizzoli, C. *Inorg. Chem.* **2005**, *44*, 9852. (i) Bergami, C.; Donzello, M. P.; Monacelli, F.; Ercolani, C.; Kadish, K. M.; Rizzoli, C. *Inorg. Chem.* **2005**, *44*, 9862. (j) Donzello, M. P.; Ou, Z.; Monacelli, F.; Ricciardi, G.; Rizzoli, C.; Ercolani, C.; Kadish, K. M. *Inorg. Chem.* **2004**, *43*, 8626. (k) Donzello, M. P.; Ou, Z.; Dini, D.; Meneghetti, M.; Ercolani, C.; Kadish, K. M. *Inorg. Chem.* **2004**, *43*, 8637. (l) Du, X.; Ma, C.; Hou, X.; Wang, G.; Li, W.; Du, G. *Heterocycles* **2003**, *60*, 2535. (m) Rusanova, J.; Pilkington, M.; Decurtins, S. *Chem. Commun.* **2002**, 2236. (n) Fox, J. M.; Katz, T. J.; Van Elshocht, S.; Verbiest, T.; Kauranen, M.; Persoons, A.; Thongpanchang, T.; Krauss, T.; Brus, L. *J. Am. Chem. Soc.* **1999**, *121*, 3453. (o) Faust, R.; Weber, C. *J. Org. Chem.* **1999**, *64*, 2571. (p) Mørkved, E. H.; Afseth, N. K.; Zimcik, P. *J. Porphyrins Phthalocyanines* **2007**, *11*, 130. (q) Mørkved, E. H.; Afseth, N. K.; Kjøsen, H. *J. Porphyrins Phthalocyanines* **2006**, *10*, 1301. (r) Angeloni, S.; Ercolani, C. *J. Porphyrins Phthalocyanines* **2000**, *4*, 474. (s) Kleinwächter, J.; Subramanian, L. R.; Hanack, M. *J. Porphyrins Phthalocyanines* **2000**, *4*, 498. (t) Mørkved, E. H.; Ossletten, H.; Kjøsen, H. *Acta Chem. Scand.* **1999**, *53*, 1117.

(12) Frisch, M. J.; Trucks, G. W.; Schlegel, H. B.; Scuseria, G. E.; Robb, M. A.; Cheeseman, J. R.; Montgomery, J. A., Jr.; Vreven, T.; Kudin, K. N.; Burant, J. C.; Millam, J. M.; Iyengar, S. S.; Tomasi, J.; Barone, V.; Mennucci, B.; Cossi, M.; Scalmani, G.; Rega, N.; Petersson, G. A.; Nakatsuji, H.; Hada, M.; Ehara, M.; Toyota, K.; Fukuda, R.; Hasegawa, J.; Ishida, M.; Nakajima, T.; Honda, Y.; Kitao, O.; Nakai, H.; Klene, M.; Li, X.; Knox, J. E.; Hratchian, H. P.; Cross, J. B.; Bakken, V.; Adamo, C.; Jaramillo, J.; Gomperts, R.; Stratmann, R. E.; Yazyev, O.; Austin, A. J.; Cammi, R.; Pomelli, C.; Ochterski, J. W.; Ayala, P. Y.; Morokuma, K.; Voth, G. A.; Salvador, P.; Dannenberg, J. J.; Zakrzewski, V. G.; Dapprich, S.; Daniels, A. D.; Strain, M. C.; Farkas, O.; Malick, D. K.; Rabuck, A. D.; Raghavachari, K.; Foresman, J. B.; Ortiz, J. V.; Cui, Q.; Baboul, A. G.; Clifford, S.; Cioslowski, J.; Stefanov, B. B.; Liu, G.; Liashenko, A.; Piskorz, P.; Komaromi, I.; Martin, R. L.; Fox, D. J.; Keith, T.; Al-Laham, M. A.; Peng, C. Y.; Nanayakkara, A.; Challacombe, M.; Gill, P. M. W.; Johnson, B.; Chen, W.; Wong, M. W.; Gonzalez, C.; Pople, J. A. *Gaussian 03*, revision D.01; Gaussian, Inc.: Pittsburgh, PA, 2004.

(13) Tokita, S.; Kojima, M.; Kai, N.; Koguri, K.; Nishi, H.; Tomoda, H.; Saito, S.; Shiraishi, S. *Nippon Kagaku Kaishi* **1990**, 219.

(14) Barbe, W.; Beckhaus, H.-D.; Lindner, H.-J.; Rüchardt, C. *Chem. Ber* **1983**, *116*, 1017.

(ESI): *m*/*z* 703.3241 ([M + H$^+$] for **3**); calcd, 703.3238. ^{1}H NMR (C_7D_8): for **1**, δ 1.53 (CH_3), 1.63 (CH_3), 1.72 (CH_3), 3.00 (CH_2); for **2**, δ 1.53 (CH_3), 1.63 (CH_3), 3.00 (CH_2); for **3**, δ 1.26 (CH_3), 1.42 (CH_3), 1.47 (CH_3), 1.59 (CH_3), 2.90 (CH_2).

Nickel β,β,β′,β′-Tetramethyl[tris-2,3-pyridino]tetraazachlorin (NiTPy^{2,3}TAC, 4a−d), Nickel β,β,β′,β′,β″,β″,β‴,β‴-Octamethyl[bis-2,3-pyridino]tetraazabacteriochlorin (NiDPy2,3TABC, 5a,b), Nickel β,β,β′,β′,β″,β″,β‴,β‴-Octamethyl[bis-2,3-pyridino]tetraazaisobacteriochlorin (NiDPy2,3TAiBC, 6a−c). A mixture of tetramethylsuccinonitrile (0.94 g, 6.9 mmol), 2,3-dicyanopyridine (0.30 g, 2.3 mmol), and anhydrous $NiCl_2$ (0.59 g, 4.6 mmol) was reacted in the presence of ammonium molybdate in boiling quinoline (5 mL) under argon for 20 min. After cooling, the reaction mixture was diluted with 20% acetone (100 mL), and the resultant precipitate was collected by filtration and washed with hot water and 20% acetone. The crude product was purified by column chromatography (silica, CH_2Cl_2), to give three fractions with R_f values of 0.64 (**5**, 6 mg, 0.9%, dark blue), 0.48 (**6**, 14 mg, 2%, pink), and 0.08 (**4**, 63 mg, 14%, blue). Each fraction was further purified by gel permeation chromatography (Bio-Beads S-x1, Biorad, $CHCl_3$). The four, two, and three possible structural isomers were separated for **4**, **5**, and **6**, respectively, by repeated silica gel TLC procedures using 10:1 (for **4**) or 15:1 (for **5** and **6**) $CHCl_3$/MeOH as the eluent. HRMS (ESI): *m*/*z* 604.1228 (**4**-1fr), 604.1224 (**4**-2fr), 604.1226 (**4**-3fr), 604.1225 (**4**-4fr) ([M + Na$^+$] for **4**); calcd, 604.1227. HRMS (ESI): *m*/*z* 611.1898 (**5**-1fr), 611.1897 (**5**-2fr) ([M + Na$^+$] for **5**); calcd, 611.1901. HRMS (ESI): *m*/*z* 611.1900 (**6**-1fr), 611.1899 (**6**-2fr), 611.1900 (**6**-3fr) ([M + Na$^+$] for **6**); calcd, 611.1901. ^{1}H NMR: for **4**-1fr, δ (10:1 $CDCl_3$/CD_3OD) 1.73 (CH_3), 1.79 (CH_3), 7.86−7.94 (3H, Ar), 9.24−9.29 (4H, Ar), 9.55−9.59 (2H, Ar); for **4**-2fr, δ (10:1 $CDCl_3$/CD_3OD) 1.80 (CH_3), 7.84−7.86 (1H, Ar), 7.90−7.94 (2H, Ar), 9.23−9.28 (3H, Ar), 9.34−9.37 (2H, Ar), 9.55−9.57 (1H, Ar); for **4**-3fr, δ (10:1 $CDCl_3$/CD_3OD) 1.76 (CH_3), 1.82 (CH_3), 7.70 (1H, Ar), 7.83−7.91 (2H, Ar), 9.08 (1H, Ar), 9.16−9.20 (2H, Ar), 9.25−9.28 (3H, Ar); for **4**-4fr, δ (10:1 $CDCl_3$/CD_3OD) 1.75 (CH_3), 7.76−7.77 (1H, Ar), 7.87−7.88 (2H, Ar), 9.09 (1H, Ar), 9.20 (2H, Ar), 9.27 (2H, Ar), 9.39 (1H, Ar); for **5**-1fr, δ (CD_2Cl_2) 1.69 (CH_3), 1.72 (CH_3), 7.77 (1H, Ar), 9.20 (Ar); for **5**-2fr, δ (CD_2Cl_2) 1.70 (CH_3), 1.71 (CH_3), 8.19 (Ar), 9.22 (Ar); for **6**-1fr, δ ($CDCl_3$) 1.53 (CH_3), 1.63−1.64 (CH_3), 7.63−7.68 (2H, Ar), 9.02−9.06 (2H, Ar), 9.09−9.12 (2H, Ar); for **6**-2fr, δ ($CDCl_3$) 1.50−1.60 (CH_3), 1.62−1.66 (CH_3), 7.57−7.69 (2H, Ar), 8.92−8.98 (1H, Ar), 9.08−9.16 (2H, Ar), 9.22−9.27 (1H, Ar); for **6**-3fr, δ ($CDCl_3$) 1.51 (CH_3), 1.56 (CH_3), 7.52−7.58 (2H, Ar), 8.85−8.90 (2H, Ar), 9.08−9.12 (2H, Ar).

Nickel β,β,β′,β′-Tetramethyl[tris-3,4-pyridino]tetraazachlorin (NiTPy^{3,4}TAC, 7a−d), Nickel β,β,β′,β′,β″,β″,β‴,β‴-Octamethyl[bis-3,4-pyridino]tetraazabacteriochlorin (NiDPy^{3,4}TABC, 8a,b), Nickel β,β,β′,β′,β″,β″,β‴,β‴-Octamethyl[bis-3,4-pyridino]tetraazaisobacteriochlorin (NiDPy^{3,4}TAiBC, 9a−c). A mixture of tetramethylsuccinonitrile (0.91 g, 6.7 mmol), 3,4-pyridinedicarboximide (0.50 g, 3.4 mmol), anhydrous $NiCl_2$ (0.88 g, 6.8 mmol), and urea (0.6 g, 10 mmol) was reacted in the presence of ammonium molybdate in boiling sulfolane (5 mL) under argon for 2 h. After cooling, the reaction mixture was diluted with water and the resultant precipitate collected by filtration and washed with hot water and hot 50% ethanol. The crude residue was transferred to a Soxhlet apparatus and successively extracted with CH_2Cl_2 and pyridine. The CH_2Cl_2 solution was concentrated to ca. 10 mL and purified by column chromatography (silica, 2:1 ethyl acetate/CH_2Cl_2 (v/v)). Three fractions with R_f values of 0.77, 0.54, and 0.19 were collected and recrystallized from $CHCl_3$/methanol to give 10 mg (1.1%) of **8** as a pink solid, 100 mg (11%) of **9** as a blue solid, and 12 mg (2.0%) of **7** as a dark blue solid. Similarly, the pyridine solution was concentrated to ca. 10 mL and purified by column chromatography (silica, 5:1 $CHCl_3$/pyridine (v/v)). A major blue portion was collected and recrystallized from $CHCl_3$/MeOH, to give 135 mg (28%) of **7**. The four, two, and three possible structural isomers were separated for **7**, **8**, and **9**, respectively, by repeated silica gel TLC procedures using 20:1 (for **7**) or 15:1 (for **8** and **9**) $CHCl_3$/MeOH as the eluent. HRMS (ESI): *m*/*z* 582.1407 (**7**-1fr), 582.1407 (**7**-2fr), 582.1406 (**7**-3fr), 582.1404 (**7**-4fr) ([M + H$^+$] for **7**); calcd, 582.1408. HRMS (ESI): *m*/*z* 589.2082 (**8**-1fr), 589.2081 (**8**-2fr) ([M + H$^+$] for **8**); calcd, 589.2081. HRMS (ESI): *m*/*z* 589.2079 (**9**-1fr), 589.2078 (**9**-2fr), 589.2078 (**9**-3fr) ([M + H$^+$] for **9**); calcd, 589.2081. ^{1}H NMR: for **7**-1fr, δ ($CDCl_3$) 1.83 (12H, CH_3), 8.79−8.80 (1H, Ar), 8.89−8.92 (2H, Ar), 9.05−9.06 (1H, Ar), 9.23−9.26 (2H, Ar), 10.25 (2H, Ar), 10.29 (1H, Ar); for **7**-2fr, δ ($CDCl_3$) 1.85 (6H, CH_3), 1.87 (6H, CH_3), 8.60−8.63 (1H, Ar), 8.74−8.78 (1H, Ar), 8.84−8.85 (1H, Ar), 8.91 (1H, Ar), 9.02−9.25 (2H, Ar), 10.08−10.10 (1H, Ar), 10.22−10.28 (2H, Ar); for **7**-3fr, δ ($CDCl_3$) 1.84 (6H, CH_3), 1.85 (6H, CH_3), 8.70−8.74 (1H, Ar), 8.78−8.81 (1H, Ar), 8.80−8.90 (1H, Ar), 8.98−9.01 (1H, Ar), 9.21−9.27 (2H, Ar), 10.20 (1H, Ar), 10.25 (1H, Ar), 10.32−10.34 (1H, Ar); for **7**-4fr, δ ($CDCl_3$) 1.87 (12H CH_3), 8.65 (1H, Ar), 8.78−8.80 (2H, Ar), 8.93 (1H, Ar), 9.22 (2H, Ar), 10.09 (1H, Ar), 10.28−10.33 (2H, Ar); for **8**-1fr, δ ($CDCl_3$) 1.63 (CH_3), 1.67 (CH_3), 8.72 (2H, Ar), 9.04 (2H, Ar), 10.21 (2H, Ar); for **8**-2fr, δ ($CDCl_3$) 1.68 (CH_3), 1.70 (CH_3), 8.73−8.74 (2H, Ar), 9.04−9.06 (2H, Ar), 10.21 (2H, Ar); for **9**-1fr, δ ($CDCl_3$) 1.53 (CH_3), 1.60 (CH_3), 8.52 (2H, Ar), 8.88 (2H, Ar), 9.91 (2H, Ar); for **9**-2fr, δ ($CDCl_3$) 1.53 (CH_3), 1.58 (CH_3) 1.60 (CH_3), 8.42 (1H, Ar), 8.57 (1H, Ar), 8.83 (1H, Ar), 8.90 (1H, Ar), 9.94 (1H, Ar), 10.05 (1H, Ar); for **9**-3fr, δ ($CDCl_3$) 1.55 (CH_3), 1.61 (CH_3), 8.47 (2H, Ar), 8.88 (2H, Ar), 10.13 (2H, Ar).

Results and Discussion

Synthesis and Separation of the Structural Isomers. It is well-known that hydrogenated TAP derivatives are prone to losing their hydrogens.[3,15] By introducing four alkyl groups instead of hydrogen at the hydrogenated sites, the chemical stability can be increased significantly.[8] In particular, methyl groups are ideal for our purpose, due to the accessibility of the starting materials and their negligible substituent effects on the spectroscopic and electrochemical properties of the compounds. Therefore, we have employed tetramethylsuccinonitrile in order to synthesize a variety of hydrogenated Pc analogues to date. For the synthesis of pyrazine- or 2,3- or 3,4-pyridine-containing derivatives, we again used tetramethylsuccinonitrile as one of the starting materials. Mixed condensation of tetramethylsuccinonitrile and 2,3-dicyano-5,6-diethyl-1,4-pyrazine in a 3:1 molar ratio was conducted in boiling quinoline in the presence of anhydrous nickel chloride and a catalytic amount of ammonium molybdate. The crude product was first extracted with chloroform, and the three expected hydrogenated derivatives could be separated by silica gel column chromatography, to give **1**−**3** in 18, 1.0, and 2.3% yields, respectively (Scheme 2). The same reaction carried out using a 1:1 molar ratio of starting dinitriles results in a significant

(15) (a) Makarova, E. A.; Korolyova, G V.; Luk'yanets, E. A. *Russ. J. Gen. Chem.* **1999**, *69*, 1306. (b) Makarova, E. A.; Korolyova, G. V.; Luk'yanets, E. A. *Zh. Obshch. Khim.* **1999**, *69*, 1356.

Scheme 2. Synthesis of Pyrazine- (top), 2,3-Pyridine- (middle), and 3,4-Pyridine-Fused (bottom) TACs, TABCs, and TAiBCs[a]

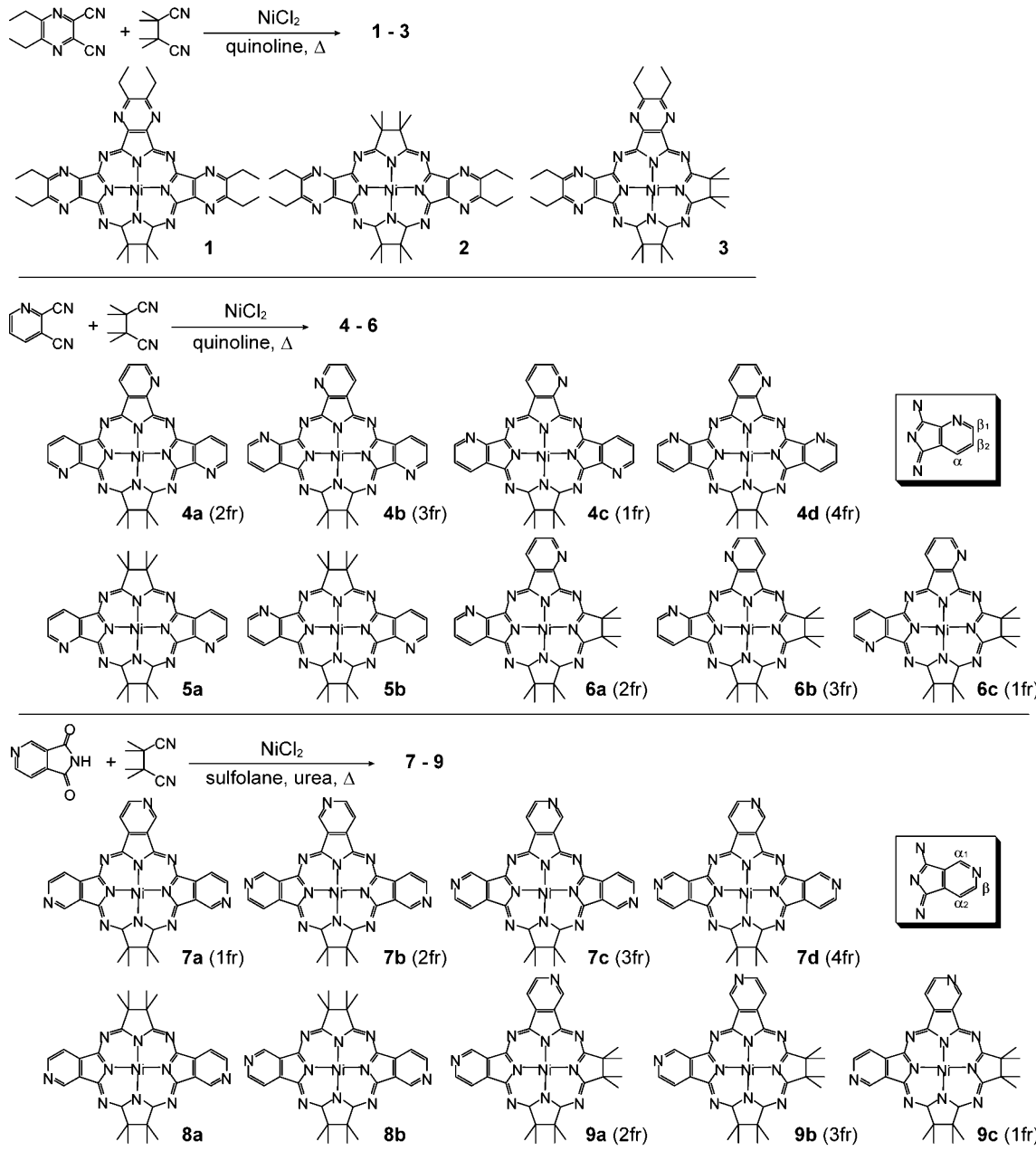

[a] Plausible assignments of the separated fractions are shown in the parentheses.

decrease in the yields of **1**−**3**. Although **2** and **3** are geometric isomers to each other, that is, two hydrogenated sites are located at the trans or cis positions of the skeleton, the observed yield of **3** is nearly double that of **2**. However, this is in good agreement with the statistically expected yields, since, when two kinds of dinitrile are annularly distributed two-by-two randomly, two and four of all possible combinations correspond to the structures of **2** and **3**, respectively. Therefore, these observations indicate that the reaction proceeds statistically.

Similar reaction conditions using 2,3-dicyanopyridine and tetramethylsuccinonitrile gave a mixture of **4**−**6** in 14, 0.9, and 2.0% yields, respectively. There are four, two, and three structural isomers for **4**, **5**, and **6**, respectively (Scheme 2). In contrast, a small amount of **7** in addition to Ni-3,4-PyTAP was obtained when 3,4-dicyanopyridine was used for the reaction. When the molar ratio of tetramethylsuccinonitrile to 3,4-dicyanopyridine was increased to 8:1, the yield of **7** increased to 10%, although **8** and **9** were detected only spectroscopically. The best results were achieved when a mixture of pyridine-3,4-dicarboximide and tetramethylsuccinonitrile in a 1:2 molar ratio was reacted in the presence of anhydrous nickel chloride, urea, and ammonium molybdate in boiling sulfolane. Thus, the best yields for **7**−**9** were 30, 1.1, and 11%, respectively. Each of the possible structural isomers was separated successfully by using repeated TLC. For example, **6a**−**6c** can be isolated by silica gel TLC (Merck, 1:2 toluene/ethyl acetate (v/v)) with R_f values of 0.57, 0.47, and 0.35, respectively. Similarly, as shown in Figure 1 (left), the TLC development (10:1 $CHCl_3$/MeOH)

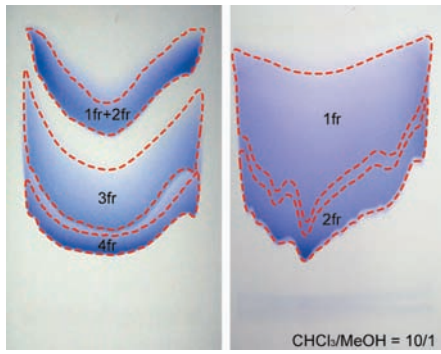

Figure 1. TLC development of **4** using a silica plate with 10:1 $CHCl_3$/MeOH (v/v) as an eluent. The first development gave three bands, in which the first band contained **4**-1fr and **4**-2fr. Complete isolation was successfully made by the second development of this band using the same conditions.

of the mixture of **4a**−**4d** gave three blue fractions, in which the first fraction (the largest R_f) contains a further two isomers. The second development of the first fraction using the same conditions gave the isolated first and second fractions (designated by 1fr and 2fr in Figure 1 (right)). The structural relationship between the obtained compounds and the structures shown in Scheme 2 is determined on the basis of the NMR spectroscopy. The ^{1}H NMR spectra of the three isomers of compound **6** (**6a**−**6c**, Figure 2 (bottom)) show that the spectral structure of **6**-2fr is more complicated than that of the other two spectra, indicating that this fraction corresponds to **6a**, since **6b** and **6c** have higher molecular symmetry elements along the diagonal containing two *meso*-nitrogen atoms located between the fused pyridine rings. It is difficult, however, to distinguish **6b** and **6c** by using the ^{1}H NMR spectra only. We assigned, therefore, **6**-1fr and -3fr as **6c** and **6b**, respectively, by combination of the spectroscopic data and DFT calculation results, as described in detail in the subsequent section. Figure 2 (top) shows that four different spectral shapes arise from the four isolated fractions of **4**, which demonstrates that the separation of the four isomers was successfully achieved. However, it is difficult to determine the isomeric structures of these. Unlike 1,2-naphtho-fused derivatives, steric congestions between the proximate fused-rings cannot be expected for the present complexes. Therefore, structural assignments using NOE experiments are less effective. Nevertheless, it is possible to propose the possible assignments of the structures on the basis of the spectroscopic evidence. Since **4**-1fr and **4**-3fr show split methyl signals, and **4**-2fr and **4**-4fr have single methyl components (not shown in Figure 2, see Experimental Section), it is plausible that **4**-1fr, **4**-3fr, **4**-2fr, and **4**-4fr are assigned as **4b**, **4c**, **4a**, and **4d**, respectively. The structure of **4**-2fr is probably that of **4a**, because the methyl signal of **4**-2fr appears further downfield compared to that of **4**-4fr (1.80 and 1.75 ppm, respectively) due to the two proximate pyridyl nitrogen atoms. The ^{1}H NMR spectrum of **4**-1fr shows a characteristic signal at ca. 9.57 ppm, which is likely to arise from the H_α affected by the pyridyl nitrogen atoms.

Since all H_α's of **4b** are separately placed from the pyridyl nitrogens, and two of three H_α's of **4c** have proximate pyridyl nitrogen atoms, it is likely that **4**-1fr and **4**-3fr correspond

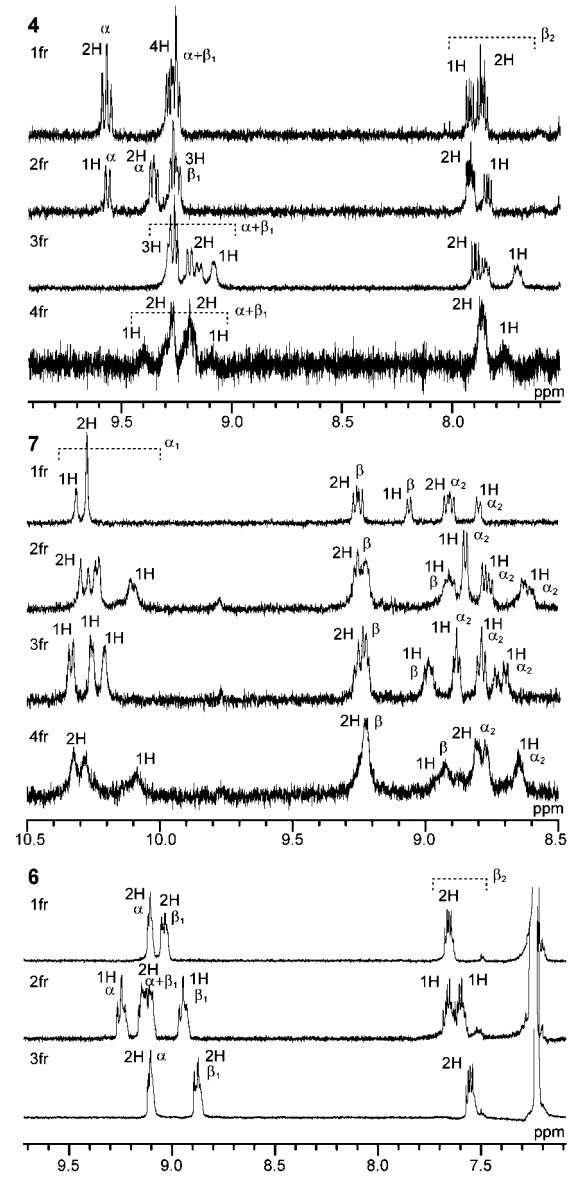

Figure 2. Aromatic region of ^{1}H NMR spectra of **4** (top), **7** (middle), and **6** (bottom).

to **4c** and **4b**, respectively. Compound **7** was similarly separated into the four isomers using TLC (silica, 20:1 $CHCl_3$/MeOH). Since **7**-2fr and **7**-3fr show split methyl signals, while **7**-1fr and **7**-4fr have single methyl components, **7**-1fr and **7**-4fr and **7**-2fr and **7**-3fr can be assigned as **7a** or **7d** and **7b** or **7c**, respectively. The signals in the 10.09−10.33 ppm region arise from the $H_{\alpha 1}$'s. Therefore, the ^{1}H NMR spectrum of **7**-1fr indicates that this molecule contains two chemically practically equivalent $H_{\alpha 1}$'s, while **7**-4fr does not. Since the $H_{\alpha 1}$'s of **7a** are placed in a chemically very similar environment compared to those of **7d**, **7**-1fr and **7**-4fr are likely assigned as **7a** and **7d**, respectively. The structure of **7d** is characterized by the fact that two of the three pyridyl nitrogen atoms point inward. This type of structure is also recognized for **7b**. As a consequence, the spectral similarities between **7**-2fr and **7**-4fr in the 10.09−10.33 ppm region imply that **7**-2fr and **7**-3fr correspond to **7b** and **7c**, respectively. The ^{1}H−^{1}H COSY spectrum also supports these

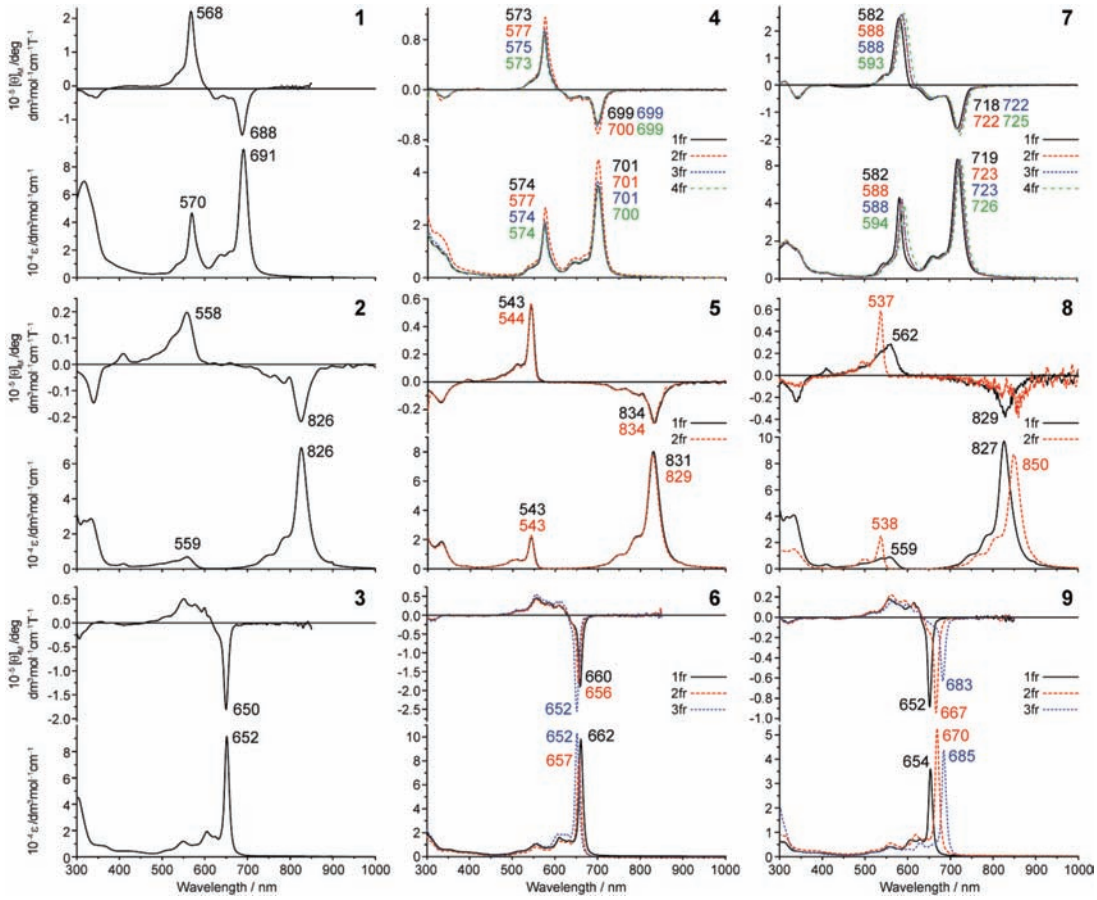

Figure 3. MCD (top) and absorption (bottom) spectra of **1**−**9** in chlorobenzene. Note that the molar coefficients of **7** were normalized to that obtained from the mixture of isomers.

assignments; that is, the signals at 10.25 and 10.29 ppm show no ^{1}H−^{1}H correlations, indicating that these arise from $H_{\alpha 1}$'s (Supporting Information). The other possible assignments are also given in Figure 2. In the case of **7**-1fr, signals at ca. 9.05 (1H) and 9.24 (2H) ppm correspond to the H_β's, since the corresponding ^{1}H signals for isoquinoline appear at 8.50 ppm in $CDCl_3$ and that of $H_{\alpha 2}$ at 7.55 ppm. The spectra of **4** show six protons in the 9.0−9.7 ppm region, indicating that the H_α's and $H_{\beta 1}$'s appear in this region. For example, the signal at 9.57 ppm of **4**-1fr evidently comes from two of the three H_α's. As shown in the COSY spectrum (Supporting Information), this signal has a correlation with the signal in the 7.86−7.94 ppm region. Therefore, the signals appearing in the 7.7−8.0 ppm region of **4** can be assigned as the $H_{\beta 2}$'s. A spectral comparison between **6** and the ^{1}H NMR spectrum of the previously reported tribenzo-fused TAC[8a] also gave information on the assignments, as indicated in Figure 2. Unfortunately, it was difficult to distinguish between **5a** and **5b** and between **8a** and **8b** using their ^{1}H NMR spectra. The structural assignments of **9** were done in a similar manner to that of **6**, that is, **9**-1fr and -3fr were assigned as **9c** and **9b**, respectively.

Electronic Absorption and MCD Spectroscopy. As described in the Introduction, the spectroscopic properties of TACs, TABCs, and TAiBCs are characterized by intense absorption bands in the visible to near-infrared region. Figure 3 shows the absorption and MCD spectra of the compounds reported in this study. Similarly to the results from our previous study, the TACs and TABCs show split Q bands, whereas the TAiBCs have single, intense Q bands.[5,7,8] Oppositely signed MCD signals corresponding to the Q-band components of the TACs and TABCs are observed, with the longer wavelength components always having a negative sign, suggesting that the energy difference between the HOMO and HOMO−1 (ΔHOMO) is larger than that of the LUMO and LUMO+1 (ΔLUMO).[16] The Soret region (ca. 300−500 nm) shows a smaller dependence on the structure and is characterized by a lower MCD intensity compared to that of the Q-band region. Although the higher-energy Q-band component of the TABCs is low in intensity, these can be assigned unambiguously by MCD spectroscopy. That is, the distinct positive MCD signals in the 500−600 nm region correspond to the higher-energy component of the split Q band. Of the split Q band of the TACs and TABCs, the band on the longer-wavelength side has a larger intensity. The splitting energy of the TABCs is larger than for the other derivatives. The largest Q-band splitting energy reaches ca. 6820 cm^{-1} for **8**-2fr, leading to a very weak corresponding MCD intensity for the longer-wavelength component of the Q band. The MCD signals corresponding to the intense Q-band components of the TAiBCs are Faraday *B* terms, which indicates that these transitions are not degenerate. Indeed, as shown in the following section, the Q band of TAiBCs actually splits into three, one of which

(16) Mack, J.; Stillman, M. J.; Kobayashi, N. *Coord. Chem. Rev.* **2007**, *251*, 429, and references therein.

is predicted to have larger intensity than the others. The shorter-wavelength components are, therefore, sufficient to be submerged in the adjacent vibronic and hot bands. Compared to the benzo-fused derivatives, the Q bands of the corresponding pyrazine- or 2,3-pyridine-fused derivatives appear on the shorter-wavelength side, while the Q-band energy of 3,4-pyridine-fused derivatives is comparable to that of the benzo-fused derivatives.[8a] The four structural isomers of **4** show very similar spectral shapes to each other. The differences in transition energy of the Q band are within 3 nm, while the MCD patterns are also practically identical. The structural dependencies of the absorption spectra in the 300−500 nm region are not significant for these compounds either. The spectra of **5**-1fr and **5**-2fr are almost identical except for slight differences in the lowest transition energy in the absorption spectra (Figure 3). The four structural isomers of **7** also show very similar spectra in shape, although the maximum differences in transition energy are somewhat larger (12 nm) compared to those of **4**. Unexpectedly, two isomers of **8** show a different Q-band energy; that is, **8**-1fr has Q-band components at 850 and 559 nm, while those of **8**-2fr lie at 827 and 537 nm. Although the bandwidth of the band at 827 nm of **8**-1fr is comparable to that of **8**-2fr, the shorter-wavelength component of **8**-1fr broadens and loses its intensity. However, since the TDDFT calculations predict that the transition energies of these two isomers are almost the same, the observed spectral differences may be attributed to molecular aggregations or other unexpected factors. The Q-band energy of the TAiBCs (**6** and **9**) depends moderately on their structures. In particular, a larger shift of the Q band, depending on the structure, was observed for **9**. The NMR study reveals that **9**-2fr (or **6**-2fr) corresponds to **9a** (**6a**); that is, the Q-band of the less symmetric compounds is located in the middle. According to our recent study,[8b] 1,2-naphtho-fused TAiBCs have a lower transition energy (i.e., the Q band appears at longer wavelengths) when two fused naphthalene rings point inward. Therefore, another isomer having two fused-naphthalene rings pointing outward has the Q band at shorter wavelengths. Judging from these considerations, it is conceivable that **9**-1fr (or **6**-3fr) and **9**-3fr (**6**-1fr) correspond to **9c** (**6c**) and **9b** (**6b**), respectively. As described in the following section, these assignments are supported also by theoretical calculations. Interestingly, despite the moderately large shift of the lowest transition energy for **9**, the tail observed on the shorter-wavelength side (i.e., bands in the ca. 500−650 nm region) is very similar for these three isomers. A similar trend is also observed for **6**, although the shift of the lowest-energy transition is less significant in this case.

Electrochemistry and DFT Calculations. In order to rationalize the observed absorption spectra, electrochemical measurements and (TD)DFT calculations were performed. The redox potential data are tabulated in Table 1. The data for **7** were obtained as a mixture of the four isomers. Cyclic voltammograms of all compounds except **7** indicate that the first and second reduction couples are reversible, as partially demonstrated in Figure 4. Although the first oxidation couples appear to be irreversible since the corresponding cathodic current is lost (Figure 4, black line), the red line shows that these processes are reversible if the sweep is reversed before reaching the second oxidations, indicating that the second oxidation states of these compounds are unstable. All of the observed redox processes can be defined safely as ring-centered, since general NiPc shows no metal-centered redox couples within this potential window in

Table 1. Redox Potentials/V (versus Fc^+/Fc) in *o*-DCB Containing 0.1 M TBAP

compd	second red	first red	first ox
1	−1.59	−1.21	0.50
2	−1.62	−1.23	0.09
3	−2.18	−1.58	0.20
4-1fr	−1.56	−1.21	0.50
4-2fr	−1.63	−1.29	0.43
4-3fr	−1.59	−1.20	0.51
4-4fr	−1.51	−1.12	0.57
5-1fr	−1.61	−1.25	0.05
5-2fr	−1.60	−1.25	0.05
6-1fr	−2.17	−1.62	0.15
6-2fr	−2.17	−1.62	0.15
6-3fr	−2.24	−1.61	0.20
7 (mixture)	−1.54	−1.17	-
8-1fr	−1.64	−1.22	0.10
8-2fr	−1.58	−1.19	0.07
9-1fr	−2.14	−1.55	0.26
9-2fr	−2.12	−1.58	0.19
9-3fr	−2.04	−1.52	0.18

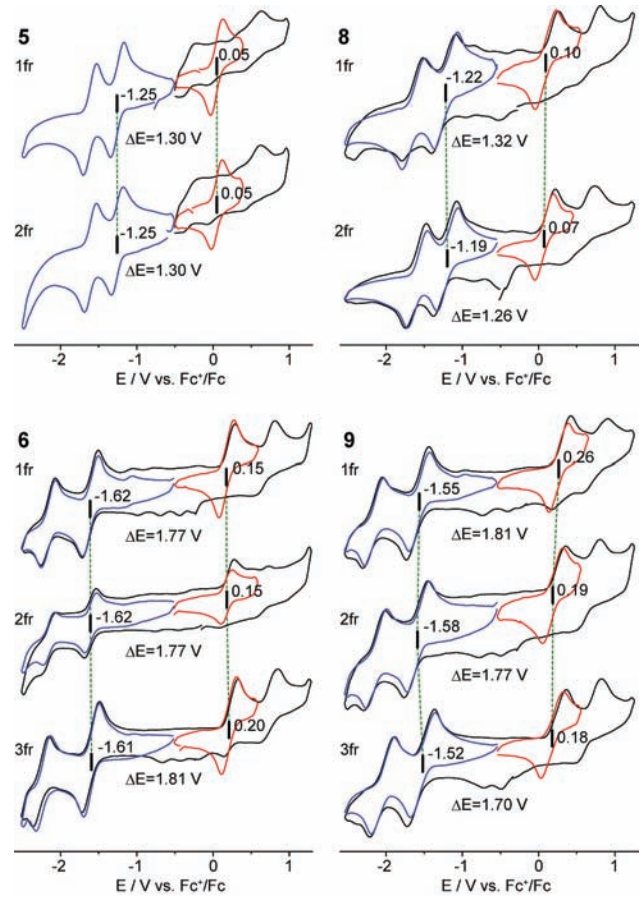

Figure 4. Cyclic voltammograms of **5** (top left), **8** (top right), **6** (bottom left), and **9** (bottom right) in *o*-DCB containing 0.1 M TBAP. The colored lines were recorded in a smaller potential window in order to confirm the reversibility of the redox processes.

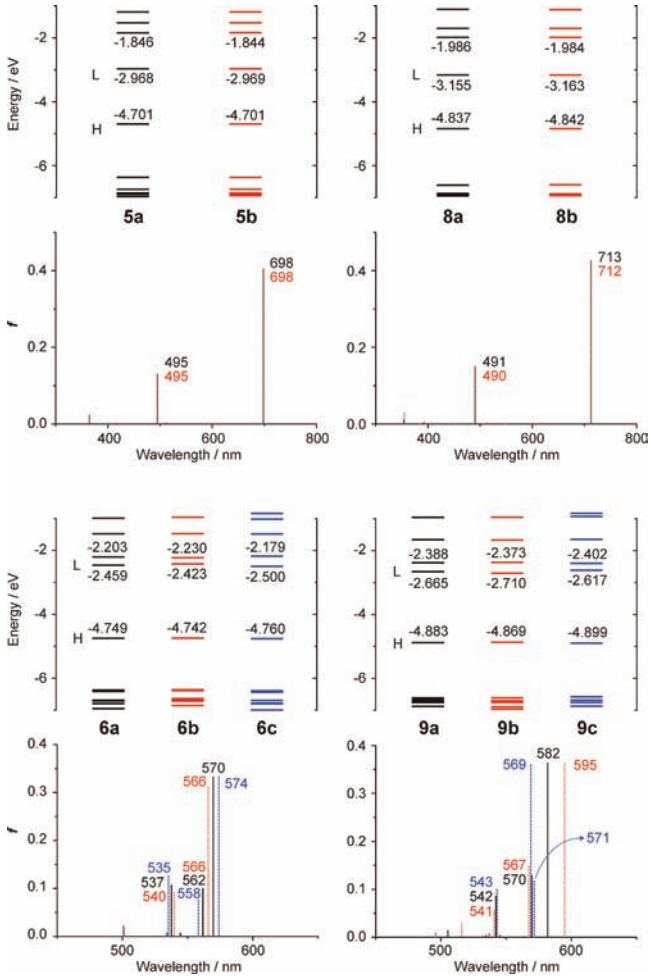

Figure 5. Partial MO energy diagram and the calculated transition energies and oscillator strengths of **5** (top left), **8** (top right), **6** (bottom left), and **9** (bottom right).

o-DCB.[17] It has been well established for Pcs that the potential differences, ΔE, between the first oxidation and first reduction potentials have a good correlation with the lowest transition energies.[18] The 3,4-pyridine-fused TAiBCs, **9**, show the first reduction and oxidation potentials at −1.55 and −1.58 V, at −1.52 V, and at 0.26, 0.19, and 0.18 V (vs Fc^+/Fc) for **9**-1fr, -2fr, and -3fr, respectively. Therefore, their ΔE values of 1.81, 1.77, and 1.70 V have a good relationship with the Q-band energies; that is, the first fraction (**9**-1fr) with the largest ΔE has the highest Q-band energy (654 nm), while **9**-3fr has the smallest potential gap and the lowest Q-band energy (685 nm). Compared to the benzo-fused derivatives, both the first oxidation and reduction potentials of the corresponding pyrazine-fused derivatives (i.e., **1**−**3**) shift cathodically, suggesting that the fused-pyrazine rings formally work as an electron acceptor, which reduces the electron density of the core skeleton of the complexes. The first reduction of the TAiBCs occurs at a much more negative potential than the TAC and TABC derivatives. On the other hand, very low oxidation potentials were observed for TABCs. These trends are comparable to those found in the benzo- and 1,2- or 2,3-naphtho-fused analogues.[7,8]

Table 2 summarizes the results of the TDDFT calculations. Both geometry optimization and TDDFT calculations were performed using the B3LYP/6-31G(d) combinations of the hybrid functional and basis set as implemented in Gaussian 03, and Figures 5 and 6 show the selected MO energy diagrams and calculated transition energies and oscillator strengths as well as the distribution of the MO coefficients, respectively. As indicated in Figure 5, two isomers of **5** and **8** were calculated to have practically identical transition energies and oscillator strengths due to the almost identical MO energies between **5a** and **5b** and between **8a** and **8b**. Since a nitrogen atom is more electronegative than a carbon atom, the MO energy is expected to be stabilized if a large MO coefficient is located on a nitrogen atom.

Figure 6 depicts that the distribution of the MO coefficients is identical between **5a** and **5b** and is symmetrical with respect to the long axis of the molecule. Therefore, the MO energies of **5a** and **5b** depend little on the positions of the nitrogen atoms, which leads to almost identical spectra in shape between **5**-1fr and **5**-2fr. In the case of TAiBCs, their HOMOs have similar energies due to the isotropic distribution of the MO coefficients (Figure 6). However, this is not the case with the LUMOs and LUMO+1's. Since the LUMOs and LUMO+1's of TAiBCs are symmetrical with respect to the diagonal, including two *meso*-nitrogen atoms, their energies depend on the location of the nitrogen atoms. For example, the calculated MO coefficients on the nitrogens of the pyridine rings are very small for the LUMO of **6b**, while those of **6c** are moderately large, leading to a more stabilized LUMO for **6c**. On the other hand, larger coefficients on the nitrogen atoms are predicted for the LUMO+1 of **6b** than for **6c**. Therefore, a more stabilized LUMO+1 was calculated for **6b**, and as a consequence, a smaller LUMO−LUMO+1 energy gap is predicted for **6b**. These interpretations also rationalize the fact that **6a** has intermediate properties between **6b** and **6c**. Conversely, in the case of **9b** and **9c**, larger coefficients on the nitrogen atoms are calculated for the LUMO of **9b** and LUMO+1 of **9c**, resulting in a larger HOMO−LUMO energy gap for **9c**.

The calculated Q bands of **1** at 602 and 520 nm consist mainly of the HOMO (150) to LUMO (151) or HOMO to LUMO+1 (152) transitions (Table 2). Similarly, the Q bands of **2** and **3** can also be attributed to the HOMO to LUMO (LUMO+1) transitions. Although the band calculated at 554 nm for **3** consists of the HOMO−3 (151) to LUMO+2 (157), HOMO (154) to LUMO+1 (156), and HOMO (154) to LUMO+2 (157) transitions, the oscillator strength of this band is small ($f = 0.04$ compared to 0.29 and 0.15 for the other Q bands). The Q bands of the pyridine-fused TACs (**4** and **7**) and TABCs (**5** and **8**) are also dominated by the HOMO to LUMO (LUMO+1) transitions. In the case of pyridine-fused TAiBCs (**6** and **9**), the most intense absorption bands consist mainly of the HOMO (154) to LUMO (155) transitions, and therefore these can be assigned as one of the split Q-band components. However, there are two

(17) Lever, A. B. P.; Milaeva, E. R.; Speier, G. In *Phthalocyanines: Properties and Applications*; Leznoff, C. C., Lever, A. B. P., Eds.; VCH: New York, 1993; Vol. *3*, Chapter 1.

(18) (a) For example: Kobayashi, N.; Fukuda, T. *J. Am. Chem. Soc.* **2002**, *124*, 8021. (b) Kobayashi, N.; Miwa, H.; Nemykin, V. *J. Am. Chem. Soc.* **2002**, *124*, 8007.

Table 2. Selected Transition Energies and Wavefunctions Calculated by the TDDFT (B3LYP/6-31G(d)) Method[a]

	λ/nm	*f*	wavefunction
1	602	0.35	0.597|151 ← 150⟩ + 0.150|152 ← 142⟩ +...
	520	0.19	0.618|152 ← 150⟩ − 0.186|151 ← 142⟩ + 0.113|155 ← 150⟩ +...
2	693	0.38	0.557|155 ← 154⟩ − 0.116|156 ← 147⟩ +...
	527	0.08	0.640|156 ← 154⟩ + 0.172|155 ← 147⟩ − 0.106|159 ← 154⟩ +...
3	567	0.29	0.589|155 ← 154⟩ + 0.137|156 ← 147⟩ − 0.105|159 ← 154⟩ +...
	554	0.04	0.343|157 ← 151⟩ − 0.316|156 ← 154⟩ − 0.304|157 ← 154⟩ +...
	529	0.15	0.547|156 ← 154⟩ + 0.244|157 ← 151⟩ + 0.157|157 ← 146⟩ − 0.130|155 ← 147⟩ +...
4a	612	0.38	0.600|151 ← 150⟩ + 0.105|152 ← 144⟩ +...
	520	0.24	0.609|152 ← 150⟩ + 0.136|151 ← 141⟩ − 0.130|151 ← 144⟩ + 0.101|151 ← 145⟩ +...
4b	614	0.38	0.595|151 ← 150⟩ − 0.104|152 ← 144⟩ +...
	519	0.24	0.610|152 ← 150⟩ − 0.131|151 ← 141⟩ + 0.126|151 ← 144⟩ +...
4c	613	0.38	0.600|151 ← 150⟩ − 0.119|152 ← 145⟩ +...
	519	0.24	0.609|152 ← 150⟩ + 0.144|151 ← 145⟩ − 0.132|151 ← 141⟩ +...
4d	614	0.39	0.595|151 ← 150⟩ + 0.121|152 ← 144⟩ +...
	518	0.23	0.609|152 ← 150⟩ − 0.146|151 ← 144⟩ + 0.125|151 ← 141⟩ +...
5a	698	0.40	0.557|155 ← 154⟩ +...
	495	0.13	0.630|156 ← 154⟩ − 0.157|155 ← 146⟩ + 0.142|155 ← 149⟩ + 0.101|155 ← 150⟩ +...
5b	698	0.40	0.557|155 ← 154⟩ +...
	495	0.13	0.631|156 ← 154⟩ + 0.156|155 ← 146⟩ − 0.135|155 ← 149⟩ + 0.124|155 ← 150⟩ +...
6a	570	0.33	0.587|155 ← 154⟩ + 0.129|156 ← 147⟩ +...
	562	0.10	0.459|156 ← 154⟩ − 0.317|157 ← 154⟩ − 0.243|157 ← 153⟩ − 0.172|146 ← 157⟩ +...
	538	0.11	0.424|156 ← 154⟩ + 0.324|157 ← 153⟩ + 0.223|157 ← 146⟩ + 0.156|157 ← 154⟩ +...
6b	566	0.14	0.469|156 ← 154⟩ + 0.286|157 ← 154⟩ − 0.204|157 ← 153⟩ + 0.187|155 ← 154⟩ +...
	566	0.31	0.557|155 ← 154⟩ − 0.157|156 ← 154⟩ + 0.109|156 ← 147⟩ +...
	540	0.09	0.385|156 ← 154⟩ + 0.339|157 ← 153⟩ + 0.250|157 ← 146⟩ − 0.210|157 ← 154⟩ +...
6c	574	0.33	0.587|155 ← 154⟩ + 0.136|156 ← 147⟩ +...
	558	0.08	0.409|156 ← 154⟩ + 0.331|157 ← 154⟩ − 0.291|157 ← 153⟩ − 0.189|157 ← 146⟩ +...
	535	0.13	0.40|156 ← 154⟩ + 0.317|157 ← 153⟩ + 0.200|157 ← 146⟩ + 0.118|157 ← 141⟩ +...
7a	631	0.41	0.594|151 ← 150⟩ + 0.107|152 ← 140⟩ + 0.104|152 ← 142⟩ +...
	524	0.27	0.610|152 ← 150⟩ − 0.144|151 ← 140⟩ − 0.140|151 ← 142⟩ +...
7b	656	0.40	0.593|151 ← 150⟩ − 0.103|152 ← 142⟩ + 0.101|152 ← 140⟩ +...
	529	0.27	0.604|152 ← 150⟩ − 0.140|151 ← 140⟩ + 0.104|151 ← 142⟩ +...
7c	635	0.41	0.593|151 ← 150⟩ − 0.112|152 ← 142⟩ +...
	530	0.27	0.606|152 ← 150⟩ + 0.163|151 ← 142⟩ +...
7d	640	0.40	0.592|151 ← 150⟩ + 0.100|152 ← 140⟩ +...
	536	0.26	0.597|152 ← 150⟩ − 0.119|151 ← 143⟩ − 0.116|151 ← 140⟩ + 0.112|151 ← 142⟩ +...
8a	713	0.43	0.553|155 ← 154⟩ − 0.121|156 ← 147⟩ +...
	490	0.15	0.629|156 ← 154⟩ + 0.200|155 ← 147⟩ − 0.132|155 ← 146⟩ +...
8b	712	0.43	0.553|155 ← 154⟩ − 0.111|156 ← 148⟩ +...
	490	0.15	0.629|156 ← 154⟩ + 0.181|155 ← 148⟩ + 0.161|155 ← 146⟩ +...
9a	582	0.36	0.589|155 ← 154⟩ + 0.129|156 ← 145⟩ +...
	570	0.13	0.513|156 ← 154⟩ + 0.304|157 ← 154⟩ − 0.195|157 ← 153⟩ +...
	542	0.09	0.365|156 ← 154⟩ + 0.345|157 ← 153⟩ − 0.248|157 ← 154⟩ + 0.166|157 ← 148⟩ +...
9b	595	0.36	0.587|155 ← 154⟩ + 0.135|156 ← 146⟩ +...
	567	0.15	0.543|156 ← 154⟩ + 0.295|157 ← 154⟩ − 0.166|157 ← 153⟩ − 0.102|155 ← 146⟩ +...
	541	0.06	0.413|157 ← 153⟩ + 0.292|156 ← 154⟩ + 0.212|157 ← 144⟩ − 0.193|157 ← 154⟩ +...
9c	571	0.12	0.494|156 ← 154⟩ + 0.310|157 ← 154⟩ + 0.226|157 ← 152⟩ + 0.106|157 ← 141⟩ +...
	569	0.36	0.589|155 ← 154⟩ − 0.108|156 ← 145⟩ + 0.101|156 ← 146⟩ +...
	543	0.10	0.399|156 ← 154⟩ − 0.338|157 ← 152⟩ − 0.264|157 ← 154⟩ − 0.156|157 ← 141⟩ +...

[a] The |150⟩ and |154⟩ represent the HOMO of the TACs (**1**, **4**, **7**) and of the TABCs and TAiBCs (**2**, **3**, **5**, **6**, **8**, **9**), respectively.

transitions, which are dominated by the HOMO to LUMO+1 transitions for each isomer of **6** and **9**. For example, transitions at 562 and 538 nm for **6a** are of this type, although the HOMO (HOMO−1) to LUMO+2 transitions also contribute importantly to these transitions (Table 2). Similar trends can be seen also for the other TAiBCs. Therefore, it can be concluded that the Q band of **6** and **9** splits into two, of which one component retains a HOMO to LUMO transition character, while the other band splits further into two by mixing with the HOMO (HOMO−1) to LUMO+2

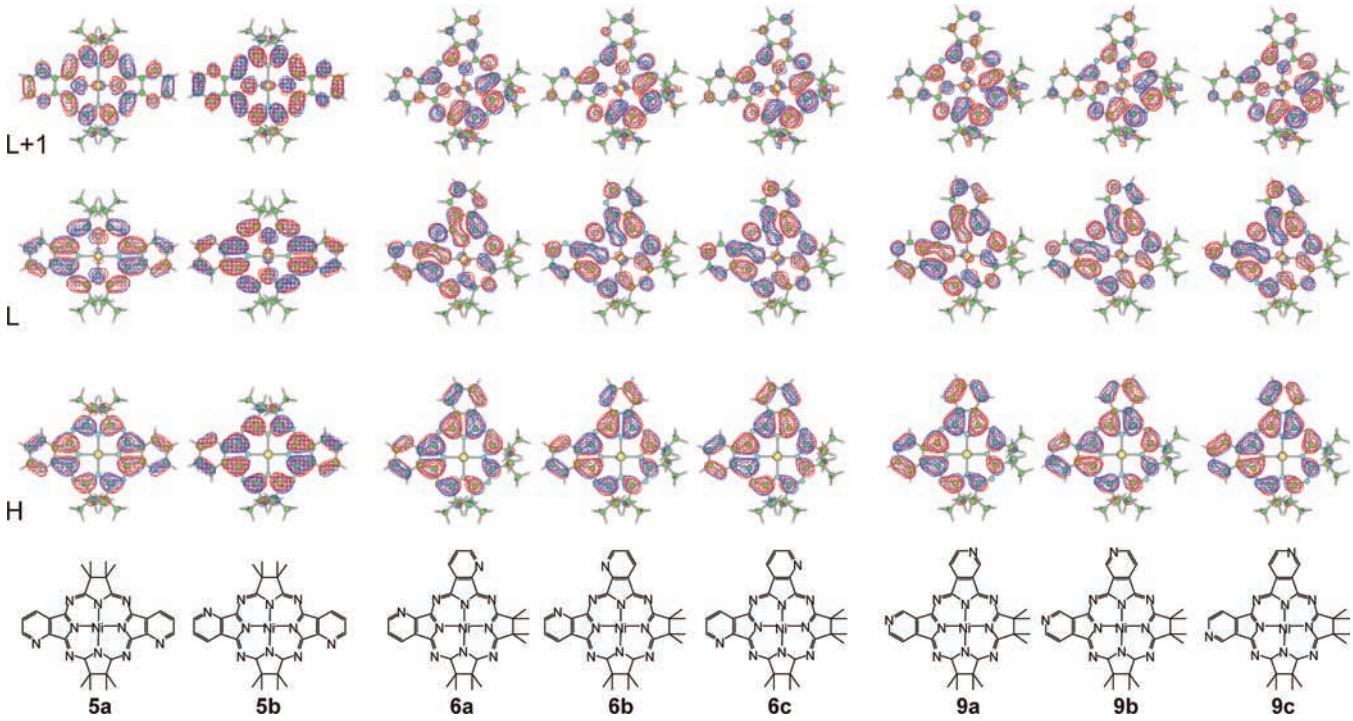

Figure 6. Amplitude of HOMO, LUMO, and LUMO+1 of **5** (left), **6** (middle), and **9** (right).

transitions. As a consequence, the resulting absorption spectra contain one intense and two less-intense Q components. Since the energy differences of the LUMO+1 among isomers are smaller than those seen for the LUMO due to the smaller MO coefficients on the fused-pyridine rings, these low-intensity split Q-band components are less affected by a change of structure, as seen in Figure 5.

Conclusions

In this study, we have synthesized novel pyrazine-, 2,3-pyridine-, and 3,4-pyridine-ring-fused tetraazachlorin, tetraazabacteriochlorin, and tetraazaisobacteriochlorin derivatives and separated all possible structural isomers by using repeated thin layer chromatography. The synthetic conditions have been carefully optimized in order to obtain the highest yields. These compounds have been characterized by various spectroscopic and electrochemical methods, including ^{1}H NMR, absorption, MCD spectroscopies, and cyclic voltammetry. Interestingly, sizable Q-band shifts were observed for the three isomers of 3,4-pyridine-fused TAiBCs, while the TACs showed no significant spectral differences between the structural isomers. The results of (TD)DFT calculations are helpful for analyzing the experimental data and rationalize the observed transition energies and intensities.

Acknowledgment. This work was supported partly by the Moscow City Government and Russian Foundation for Basic Research (Grand 08−03−90007-Bel_a), and Grant-in-Aid for Exploratory Research (No. 19655045) to NK from the Japan Society for Promotion of Science (JSPS). T.F. thanks the Intelligent Cosmos Foundation, and the Exploratory Research Program for Young Scientists from Tohoku University for their financial support. N.H. is grateful to the Sasakawa Scientific Research Grant from the Japan Science Society.

Supporting Information Available: ^{1}H−^{1}H COSY spectrum of **4**-1fr and **7**-1fr. This material is available free of charge via the Internet at http://pubs.acs.org.

IC801552U